ELSEVIER

Chemical Physics 266 (2001) 205–212

Chemical Physics

www.elsevier.nl/locate/chemphys

Cascaded free-induction decay four-wave mixing ☆

Vadim V. Lozovoy [a,1], Igor Pastirk [a,b], Matthew G. Comstock [a], Marcos Dantus [a,*]

[a] *Department of Chemistry and Center for Fundamental Materials Research, Michigan State University, East Lansing, MI 48824-1322, USA*

[b] *Institute for Nuclear Sciences "VINCA", Belgrade, F.R. Yugoslavia*

Received 16 October 2000

Abstract

We report the observation of cascaded optical free-induction decay four-wave mixing (FID-FWM) signal. This process can take place when nonlinear optical measurements are carried out with pulses that are orders of magnitude shorter than the dephasing time of the sample. Experimental observations and theoretical calculations show that the coherent emission from the first laser pulse participates as a time-delayed local electric field to yield the cascaded signal. We arrive at this conclusion based on pulse sequences of degenerate noncollinear femtosecond pulses for which three-pulse FWM is forbidden. Further confirmation was obtained from experiments where the time delay between two pulses were used to form ground or excited state populations, the signal reflected the corresponding ground or excited state dynamics. Although FID is long lived, the femtosecond resolution was found to be maintained in our measurements on gas phase molecular iodine. This is because the FID is modulated in the femtosecond time scale by the molecular dynamics of the system; its intensity and modulation were confirmed using femtosecond time-gated up-conversion measurements.

1. Introduction

In this article, we consider four-wave mixing (FWM) experiments in a regime where the dephasing time of the sample is orders of magnitude longer than the laser pulses that induce it. The polarizations generated by each laser can interact with the system long after the pulses have passed, leading to the generation of new nonlinear signals. Here we isolate these effects using pulse sequences for which three-pulse FWM processes are forbidden. This article is a continuation of efforts from our group on sorting the role of pulse sequences in the study and control of molecular dynamics in gas phase samples [1–7].

The timing between the pulses plays a crucial role in time-resolved nonlinear optical spectroscopy. The Liouville equation, describing the time evolution of the density matrix, depends on knowledge about the timing at which each laser pulse interacts with a system to generate nonlinear optical signals. Graphical representations of the Liouville equation, such as double-sided Feynman

☆ This work was first presented at the Symposium on Multidimensional Spectroscopies, APS Meeting, Minneapolis, MN, March 2000.

* Corresponding author. Tel.: +1-517-355-9715, ext. 314; fax: +1-517-353-3023/+1-517-353-1793.

E-mail address: dantus@msu.edu (M. Dantus).

[1] Permanent address: N.N. Semenov Institute of Chemical Physics, RAS, Moscow, Russian Federation.

0301-0104/01/$ - see front matter
PII: S0301-0104(01)00229-4

diagrams (DSFD) have been developed to sort out the various nonlinear optical responses to different pulse sequences [8,9]. For resonant excitation, only the diagrams that fulfil the rotating wave approximation (RWA) contribute significantly to the signal [8,9]. These descriptions of the FWM process can be used to determine the mechanism for signal formation. When the duration of the laser pulses is orders of magnitude shorter than the coherence decay of the sample additional wave-mixing phenomena involving the optical free-induction decay (FID) from the first beam can take place. The object of this study is to characterize the nature of these cascaded (C) FID-FWM processes.

We explore C-FID-FWM phenomena using pulse sequences that prevent three-pulse FWM signal formation along the detected phase-matching direction. The pulse sequences and the individual pulse wave vectors, $\boldsymbol{k}_i$, are shown diagrammatically in Fig. 1. The noncollinear laser beams are focused and overlapped at the sample. The signal is detected at the phase-matching direction $\boldsymbol{k}_s = \boldsymbol{k}_a - \boldsymbol{k}_b + \boldsymbol{k}_c$ [1,2]. Note that beams a and c are diagonally opposed in the transient grating schematic, and because of symmetry are equivalent.

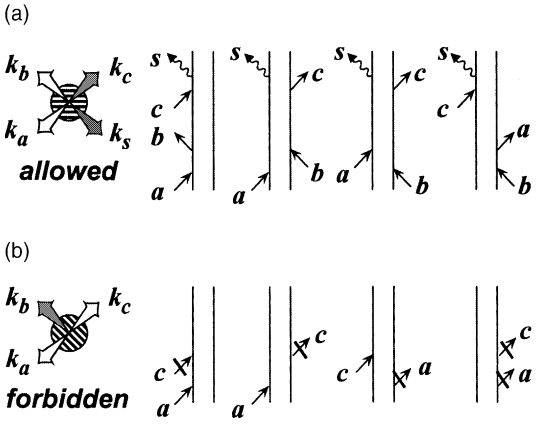

Fig. 1. (a) Transient grating diagrams and DSFD (R_4, R_1, R_2 and R_3 from left to right, respectively) for the case when pulses a and b precede pulse c. In these cases pulses a and b form a transient grating (indicated by the horizontal lines) and the signal arises from the Bragg diffraction of pulse c. (b) Transient grating and DSFD for the case when pulse b is the last to arrive at the sample. The grating formed by pulses a and c (indicated by the diagonal lines) cannot diffract pulse b in the signal direction. Violation of the RWA is identified in the DSFD by the crossed arrows.

They are represented by right-going arrows in the DSFD. Beam b bisects beams a and c, it has a negative wave vector contributions to the signal, therefore, it is represented by a left-going arrow in the DSFD. In Fig. 1(a) we give the four DSFD that are responsible for three-pulse FWM, when pulses a and b arrive at the sample before pulse c. These diagrams are applicable to FWM processes involving two electronic levels with vibrational and rotational manifolds each, and are known as responses R_4, R_1, R_2, and R_3 respectively [9]. For a three-level system, additional diagrams must be considered [10]. The first pair of diagrams in Fig. 1(a), correspond to virtual echo (or perturbed FID) sequences with $(a;-b;c)$ [8,12] and the second pair correspond to three-pulse stimulated photon echo sequences with $(-b;a;c)$ [8,9], where the order is given as (first; second; third). The diagrams in Fig. 1(b), when pulses a and c arrive at the sample before pulse b with the general pulse sequence $(a;c;-b)$, violate the RWA and are not expected to yield FWM signal.

Three-pulse FWM measurements can also be understood in terms of Bragg diffraction of the third pulse from transient grating formed by the first two pulses [11]. Transient grating schematics are shown in Fig. 1. The two beams responsible for grating formation are indicated by white arrows, the third pulse is shaded gray. The Bragg diffracted signal, with $\boldsymbol{k}_S$, is indicated by a black arrow. The transient grating schematic in Fig. 1(a) has the proper orientation for Bragg diffraction of pulse c in the phase matching direction. Fig. 1(b) shows that the transient grating resulting from the crossing of beams a and c is in a direction that cannot lead to Bragg diffraction of pulse b towards the detector. No conventional FWM signal is expected from the pulse sequences in Fig. 1(b). In this article we use the pulse sequence $(c;a;-b)$, where a and c are the first two pulses, as in Fig. 1(b), to isolate the C-FID-FWM signal.

2. Experimental

The experimental setup has been described in detail elsewhere [1,2]. Three degenerate 60 fs laser pulses centered at 620 nm, and ~30 μJ energy,

cross at the 5-cm long sample cell containing iodine vapor at 140°C (see Fig. 2(a)). The OD of the sample was kept at 0.25. The time delay between pulses a and b was fixed while the time delay between pulses b and c, indicated by $\tau = t_c - t_b$, was scanned. Accordingly, time zero is defined as the time when $\tau = t_c - t_b = 0$. The lasers are arranged in the phase-matching geometry shown in Fig. 2(a).

Femtosecond time-gated up-conversion was used to measure the FID from the experimental cell. We used the experimental arrangement depicted in Fig. 2(b). The unfocused pump laser ~25 μJ, was transmitted through the cell and was focused on a 0.5 mm KDP crystal. The gate pulse ~1 μJ, was focused on the KDP crystal and scanned in time. The second harmonic signal corresponded to the femtosecond time-gated FID, up-converted in the nonlinear crystal. The signal was filtered spatially and spectrally with a spectrometer before detection.

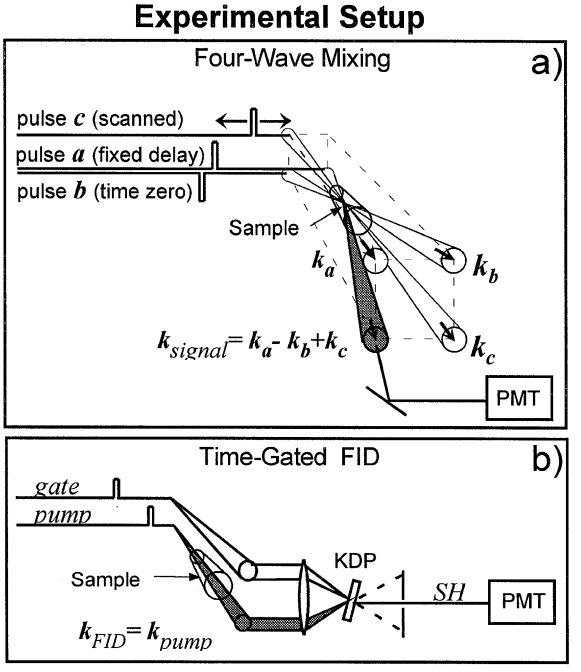

Fig. 2. (a) Experimental arrangement for FWM experiments. The laser pulses are crossed in a phase-matched geometry. The pulse arrangement shown is for experiments with a fixed time between pulses a and b. (b) Experimental arrangement used for time-gated FID measurements using femtosecond up-conversion. The pump pulse transmits through the sample and the gate pulse up-converts the FID following the pump pulse in a nonlinear optical crystal (KDP). The up-converted signal (SH) is detected by a photomultiplier after spectral and spatial filtering.

3. Results and discussion

For the first set of three-pulse FWM experiments, two pulses were overlapped in time leaving only one time delay as a variable. For the second set of experiments, the time delay between two of the pulses was used as an additional variable to help sort the nonlinear processes. In Fig. 3 we present experimental results when laser pulses a and c coincide in time and laser pulse b is scanned in time. When beam b arrives at the sample first, it (or the polarization caused by it in the sample) forms a transient grating with beam a. Beam c diffracts from this grating to form the photon echo signal (see Fig. 1(a)). However, when pulse b arrives last, no signal is expected, as discussed earlier (see Fig. 1(b)). This situation occurs for negative τ in Fig. 3. The signal observed for negative τ is relatively strong and shows femtosecond time-resolved features.

In Fig. 4 we present experiments with pulses a and b separated by a fixed time delay. When pulse

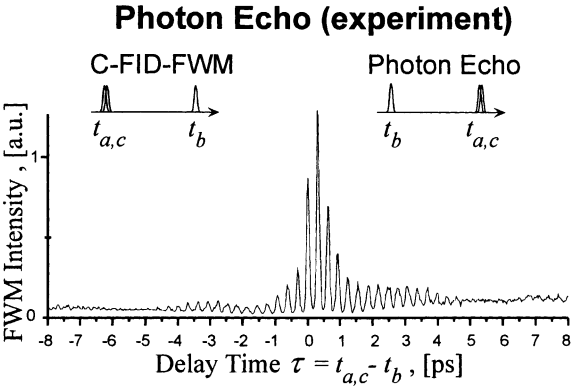

Fig. 3. Experimental FWM data obtained for pulse sequences having pulses a and c overlapped in time. For positive τ, the signal corresponds to the three-pulse photon echo phenomenon. For negative τ, the signal corresponds to the C-FID-FWM process. The modulation of the signal (307 fs) corresponds to the time-resolved vibrational dynamics of the B state of iodine.

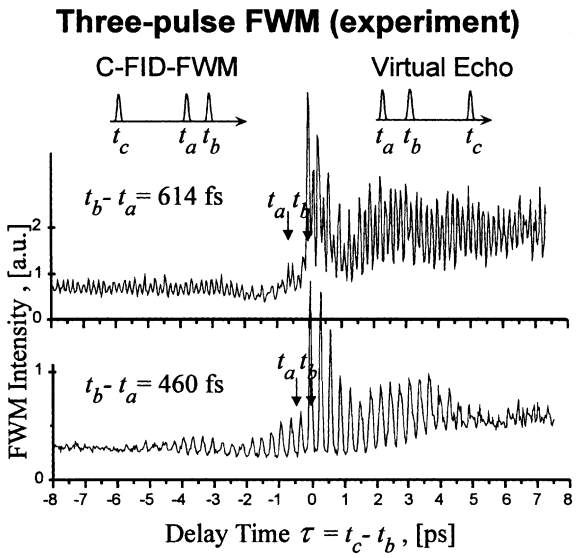

Fig. 4. Experimental FWM data obtained for pulse sequences with a fixed time-delay between pulses a and b. For positive τ, the signal corresponds to a virtual photon echo phenomenon. For negative τ, the signal corresponds to C-FID-FWM. The time delay between pulses a and b, in both cases, controls the observation of ground (upper experiment, oscillation period 160 fs) or excited electronic state motion (bottom experiment, oscillation period 307 fs).

c arrives at the sample after pulses a and b strong FWM signal, corresponding to a virtual echo phenomenon is observed [12,13]. The first two DSFD in Fig. 1(a) correspond to this observation. Pulses a and b form the grating and pulse c diffracts to form the signal. The observation of ground (160 fs oscillation period, upper experiment) or excited state (307 fs oscillation period, lower experiment) vibrational dynamics when the time delay between pulses a and b is 614 or 460 fs respectively has been discussed elsewhere [2–5]. When pulse c precedes the two other pulses, no signal is expected. Pulse c cannot diffract from a grating that has not been formed. The signal formation mechanism of this counter-intuitive pulse sequence is explained below.

The experiments shown in Figs. 3 and 4 were designed to prevent the observation of three-pulse FWM for negative τ. Violation of the RWA as observed in off-resonance FWM, could not explain this signal because it would contribute only while the three pulses are overlapped in time. Two-photon excitation, as observed in three-level systems [10], can also be ruled out because such process would reach a repulsive state in molecular iodine [14], and its short lifetime would not be consistent with our observations.

We propose that the FID, induced by the first pulse stimulates signal formation. FID is a coherent spontaneous emission that maintains the same directionality as the original pulse [15]. A portion of the molecules (ensemble 1) is excited by the first pulse c and this leads to FID. Another portion of the molecules (ensemble 2) interacts with pulses a and b forming a transient grating that diffracts the long-lived FID from ensemble 1 in the phase-matching direction. This nonlinear phenomenon is hence designated C-FID-FWM, and it is identified here as an important source of FWM signal when samples with long-lived coherence are probed with ultrafast pulses.

The experimental C-FID-FWM data obtained for negative τ in Fig. 4 arises from the diffraction of the long-lived FID induced by pulse c by the grating formed by pulses a and b. The observation of ground or excited state vibrational dynamics as a function of the time delay between pulses a and b is consistent with the proposed scheme. Note that the signal for positive and negative times is very similar except for the lower intensity in the case of negative τ. Here we highlight the fact that the FID from pulse c (a coherent emission) plays the role of a third pulse in C-FID-FWM as shown in the DSFD.

The participation of an electric field from an induced polarization in the system is not unprecedented and is referred to as cascading. However, the known cascaded processes involve a high order polarization and these processes compete with other noncascaded nonlinear processes, for example, two-photon absorption and second-harmonic generation in noncentrosymmetric crystals [16–18], or FWM processes in six-wave mixing measurements [19–21]. In contrast to the examples above, C-FID-FWM (i) involves a first-order polarization, (ii) can be observed for pulse sequences for which three-pulse FWM is forbidden, and (iii) can only take place when probing long-coherence lifetime samples with ultrafast pulses.

The intensity of C-FID-FWM can be estimated from the experimental parameters. The probability of excitation by the pulse can be approximated with $P_{\text{pulse}} \propto (E_{\text{pulse}}\tau_{\text{pulse}})^2$, where τ_{pulse} is the duration of the pulse (in our case ~50 fs) and E_{pulse} is the electric field strength of the pulse. For our experiments, approximately half the energy of the pulse $W_{\text{pulse}} \propto E^2_{\text{pulse}}\tau_{\text{pulse}}$ is absorbed. The electric field strength of FID during the first picoseconds depends on the Einstein coefficient of spontaneous emission $A \propto 1/\tau_{\text{rad}}$ (the radiative time $\tau_{\text{rad}} \sim 1$ μs for the B → X transition in iodine molecules [22–24]), therefore, $E^2_{\text{FID}} \propto W_{\text{pulse}}A \approx E^2_{\text{pulse}}\tau_{\text{pulse}}/\tau_{\text{rad}}$. The probability of excitation by the FID is limited by the coherence lifetime τ_{coh} (150 ps for our sample [25]), and is given by $P_{\text{FID}} \propto (E_{\text{FID}}\tau_{\text{coh}})^2$. The expected intensity ratio $I_{\text{C-FID-FWM}}/I_{\text{FWM}} \approx P_{\text{FID}}/P_{\text{pulse}} \approx (E_{\text{FID}}\tau_{\text{coh}})^2/(E_{\text{pulse}}\tau_{\text{pulse}})^2 \approx \tau^2_{\text{coh}}/(\tau_{\text{rad}}\tau_{\text{pulse}})^2 \approx 0.3$ is comparable with our experimental results. The estimate above helps to define the range of parameters for which C-FID-FWM can play an important role.

In order to determine experimentally the intensity, duration and modulation of the FID from our sample we carried out femtosecond up-conversion experiment with the setup shown in Fig. 2(b). The pump pulse and the FID that follows it were time-gated by an external femtosecond gate pulse. The second harmonic crystal up-converted the FID, and the resulting signal was detected. Two experimental time-gated FID measurements are presented in Fig. 5. The first scan includes the femtosecond pump pulse at time zero, and shows only the first oscillation of the FID signal. The second scan, obtained under higher sensitivity, reveals the femtosecond modulation of the FID. The oscillation period corresponds to the wave packet dynamics in the excited state as it sloshes in and out of the Frank–Condon region. These measurements confirm our assumptions about the FID in terms of intensity and femtosecond time modulation.

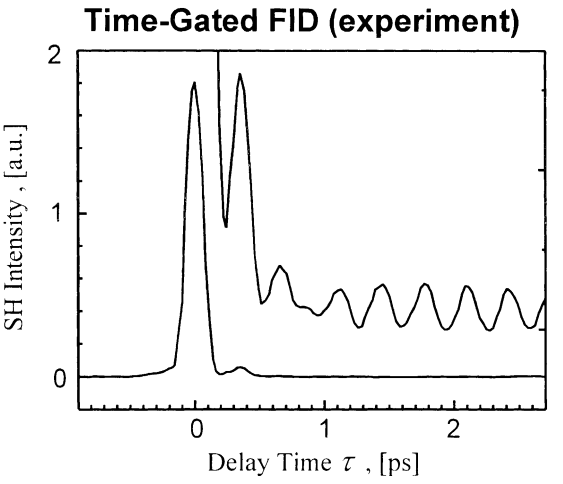

Fig. 5. Experimental time-gated FID data. The signal corresponds to the up-converted optical FID by a femtosecond gate pulse in a nonlinear optical crystal. Two different scans are shown. The first scan includes the pump pulse centered at $\tau = 0$. The second scan, obtained under higher sensitivity, shows modulations in the signal caused by the wave packet dynamics in the B state of iodine.

4. Theory

Below we give a brief theoretical description of C-FID-FWM based on the solution of the Liouville equation. Microscopic expressions for cascading are given in Chapter 16 of Ref. [9]. Evolution of the density-matrix elements ρ_{ij} in the absence of an external field can be described with the free propagator, under interaction with the vibronic matrix elements V_{ij}.

$$V^{[\alpha]}_{ij} = A^{[\alpha]}_{ij} e^{i\boldsymbol{k}_\alpha \boldsymbol{x}}, \quad \text{where } A^{[\alpha]}_{ij} = \frac{\mu_{ij}}{\hbar} S^{[\alpha]1/2}_{ij} \tag{1}$$

where the label α indicates the interacting pulse *a, b* or *c*; *i* and *j* are indices for vibrational levels in the excited and ground state respectively; ω_{ij} and μ_{ij} are the transition frequencies and dipole moment on the *ij*th transition; $S^{[\alpha]}_{ij}$ is the spectral intensity of the corresponding transition induced by the transform-limited pulse α with carrier frequency ω_0 and wave vector $\boldsymbol{k}_\alpha$; $A^{[\alpha]}_{ij}$ are the macroscopic space-independent ($\boldsymbol{x}$) components of $V^{[\alpha]}_{ij}$.

The initial condition of the density matrix $\rho^{(0)}_{jj} = n_j$ is given by a Boltzmann distribution. After pulse *c* interacts with the sample at time t_1, the induced polarization causes FID with the wave vector $\boldsymbol{k}_{\text{FID}} = \boldsymbol{k}_c$,

$$E_{\mathrm{FID}}(t) \propto \sum_i \sum_j \mu_{ij}[V_{ij}^{[c]} \mathrm{e}^{-\mathrm{i}\omega_{ij}(t-t_1)} - V_{ij}^{[c]*} \mathrm{e}^{\mathrm{i}\omega_{ij}(t-t_1)}]n_j. \tag{2}$$

This field interacts with medium, $V_{ij}^{[\mathrm{FID}]} \propto \mu_{ij} E_{\mathrm{FID}}$, after pulses a and b at times t_2 and t_3 causing the third-order polarization

$$\begin{aligned}\rho_{ij}^{(3)}(t) \propto & -\mathrm{e}^{-\mathrm{i}\omega_{ij}(t-t_3)} \sum_{j''} \rho_{j''j}^{(2)}(t_3)\mu_{ij''} \sum_{i'j'} \mu_{i'j'} \\ & \times \int_{-\infty}^{t} \mathrm{d}t' \mathrm{e}^{\mathrm{i}\omega_{ij''}(t'-t_3)} [\mathrm{e}^{-\mathrm{i}[\omega_{i'j'}(t'-t_1)-\boldsymbol{k}_{\mathrm{FID}}\boldsymbol{x}]} \\ & \quad - \mathrm{e}^{\mathrm{i}[\omega_{i'j'}(t'-t_1)-\boldsymbol{k}_{\mathrm{FID}}\boldsymbol{x}]}] A_{i'j'}^{[c]} n_{j'} \\ & \quad + \mathrm{e}^{-\mathrm{i}\omega_{ij}(t-t_3)} \sum_{i''} \rho_{ii''}^{(2)}(t_3)\mu_{i''j} \sum_{i'j'} \mu_{i'j'} \\ & \times \int_{-\infty}^{t} \mathrm{d}t' \mathrm{e}^{\mathrm{i}\omega_{i''j}(t'-t_3)} [\mathrm{e}^{-\mathrm{i}[\omega_{i'j'}(t'-t_1)-\boldsymbol{k}_{\mathrm{FID}}\boldsymbol{x}]} \\ & \quad - \mathrm{e}^{\mathrm{i}[\omega_{i'j'}(t'-t_1)-\boldsymbol{k}_{\mathrm{FID}}\boldsymbol{x}]}] A_{i'j'}^{[c]} n_{j'}. \end{aligned} \tag{3}$$

Only resonance terms can stimulate optical transitions, therefore, terms with $\omega_{ij''} = \omega_{i'j'}$ in the first sum and $\omega_{i''j} = \omega_{i'j'}$ in the second sum are kept. The second order density matrix elements, $\rho_{ij}^{(2)}$ in Eq. (3), can be calculated with the following formula applicable for well-separated pulses [26]

$$\begin{aligned}\rho_{ij}^{(n)}(t) = \mathrm{i}\mathrm{e}^{-\mathrm{i}\omega_{ij}(t-t_n)} \Bigg\{ & \sum_{i'} \Big[V_{ii'}^{[n]} \rho_{i'j}^{(n-1)}(t_n) \\ & - \rho_{ii'}^{(n-1)}(t_n) V_{i'j}^{[n]} \Big] + \sum_{j'} \Big[V_{ij'}^{[n]} \rho_{j'j}^{(n-1)}(t_n) \\ & - \rho_{ij'}^{(n-1)}(t_n) V_{j'j}^{[n]} \Big] \Bigg\}. \end{aligned} \tag{4}$$

To calculate the virtual echo and C-FID-FWM signals, we pick the nonzero density matrix elements of $\rho_{ij}^{(3)}$ proportional to $\exp[-\mathrm{i}(\omega_0 t - (\boldsymbol{k}_a - \boldsymbol{k}_b + \boldsymbol{k}_c)\boldsymbol{x})]$, because only these components emit light in the phase-matching direction. The intensity of the time-integrated signal is given by

$$I = \sum_{ij} \boldsymbol{I}_{ij}, \quad \text{where } \boldsymbol{I}_{ij} \propto \mu_{ij}^2 \int_{t_3}^{\infty} \mathrm{d}t |\rho_{ij}^{(3)}(t)|^2. \tag{5}$$

An expression to calculate the spectral components $I_{ij}^{[\mathrm{FID}]}$ of the C-FID-FWM signal observed for negative $\tau_{cb} = t_c - t_b$ can be obtained as follows. We use Eq. (4) to calculate $\rho_{ij}^{(2)}$, introduce these elements into Eq. (3), and finally, calculate each element with Eq. (5) using $\tau_{ba} = t_b - t_a$, to obtain

$$\begin{aligned} I_{ij}^{[\mathrm{FID}]} \propto \mu_{ij}^2 \Bigg| & \sum_{j'} \mathrm{e}^{\mathrm{i}\omega_{ij'}\tau_{cb}} \mu_{ij'}^2 A_{ij'}^{[c]} n_{j'} \sum_{i'} \mathrm{e}^{-\mathrm{i}\omega_{i'j}\tau_{ba}} A_{i'j'}^{[b]*} A_{i'j}^{[a]} n_j \\ & + \sum_{i'} \mathrm{e}^{\mathrm{i}\omega_{i'j}\tau_{cb}} \mu_{i'j}^2 A_{i'j}^{[c]} n_j \sum_{j'} \mathrm{e}^{-\mathrm{i}\omega_{ij'}\tau_{ba}} A_{i'j'}^{[b]*} A_{ij'}^{[a]} n_{j'} \Bigg|^2. \end{aligned} \tag{6}$$

The spectral components $I_{ij}^{[\mathrm{VE}]}$ of the three-pulse virtual echo signal for positive τ_{cb} are obtained using Eqs. (4) and (5)

$$\begin{aligned} I_{ij}^{[\mathrm{VE}]} \propto \mu_{ij}^2 \Bigg| & \sum_{j'} \mathrm{e}^{-\mathrm{i}\omega_{j'j}\tau_{cb}} A_{ij'}^{[c]} \sum_{i'} \mathrm{e}^{-\mathrm{i}\omega_{i'j}\tau_{ba}} A_{i'j'}^{[b]*} A_{i'j}^{[a]} n_j \\ & + \sum_{i'} \mathrm{e}^{-\mathrm{i}\omega_{ii'}\tau_{cb}} A_{i'j}^{[c]} \sum_{j'} \mathrm{e}^{-\mathrm{i}\omega_{ij'}\tau_{ba}} A_{i'j'}^{[b]*} A_{ij'}^{[a]} n_{j'} \Bigg|^2. \end{aligned} \tag{7}$$

Eqs. (6) and (7) are very similar. The time delay τ_{ba} is the control parameter that allows us to select between ground and excited state dynamics in both cases [2–5]. The signal is obtained as a function of the time delay τ_{cb} in both cases. Computer simulation for both cases, using the available spectroscopic data [22–24], the experimental laser parameters, and Eqs. (6) and (7), are shown in Fig. 6. Rotational dephasing effects have also been included using the formulations by Lozovoy et al. [27]. The relative amplitudes of the signals were normalized according to the estimated ratio between C-FID-FWM and conventional FWM as discussed above. The theoretical simulations shown in Fig. 6 are in agreement with the experimental data in Fig. 4.

5. Conclusion

The combination of ultrafast lasers, with samples having long coherence times can be used to yield nonlinear optical signals that are not easily

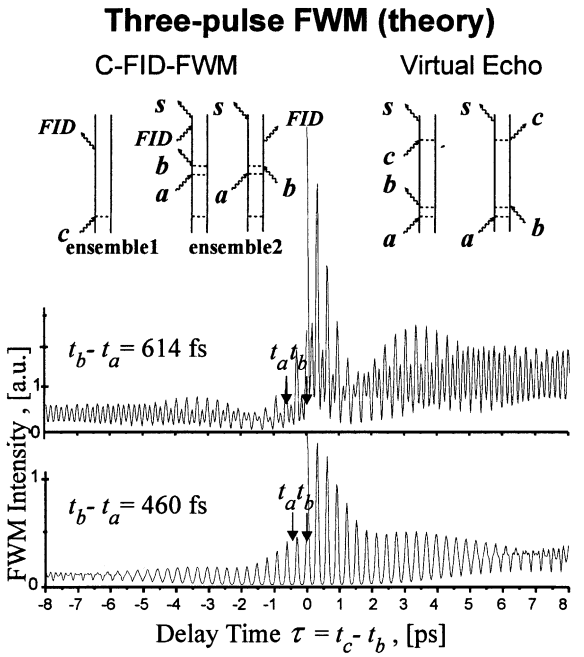

Fig. 6. Theoretical simulation of the experimental results presented in Fig. 4 without adjustable parameters. The DSFD that describe the results are also shown (top). For positive τ, the signal corresponds to a virtual photon echo phenomenon. For negative τ, the signal corresponds to C-FID-FWM. Interaction of pulse c with ensemble 1 initiates the long-lived FID with wave-vector $\boldsymbol{k}_{\mathrm{FID}} = \boldsymbol{k}_c$. The FID diffracts from the ground or excited state gratings formed by the pulses a and b in ensemble 2 and generates a coherent emission in the direction $\boldsymbol{k}_a - \boldsymbol{k}_b + \boldsymbol{k}_c$. The simulations include rotational dephasing effects.

observed with conventional laser sources. Here we present two experiments that illustrate this point and discuss the conditions required for their observation. The experiments demonstrate that FID can cause the formation of FWM signal for pulse sequences where conventional FWM is forbidden. Femtosecond up-conversion measurements confirmed the intensity and modulation of the FID, caused by the wave packet dynamics in the excited state of the sample. A theoretical formulation for the processes discussed was presented. Results from this model simulate the observed experimental results and confirm that femtosecond time resolution is maintained. The participation of FID in nonlinear optical measurements, as discussed here, is expected to be observable for any system where $\tau_{\mathrm{coh}}^2/(\tau_{\mathrm{rad}}\tau_{\mathrm{pulse}})$ is near unity. We estimate that C-FID-FWM should be observable for some condensed phase system such as a laser dye solution irradiated with sub-10 fs laser pulses. The nonlinear processes responsible for the negative time delay signal in photon echo were first discussed in the theory by Leegwater and Mukamel [28]. It is possible that Kinrot and Prior observed this effect when analyzing the photon echo signal from a sample at high concentration [29]. After the preparation of this manuscript we learned that a similarly forbidden FWM signal was observed in a dense atomic vapor, and explained as a Lorentz local-field effect [30].

Acknowledgements

We want to thank Professor Shaul Mukamel for insightful comments on this observation and Dr. Bruna Grimberg for a critical review of this manuscript. This research was partially funded by a grant from the NSF (CHE-9812584). MD is a Lucille and David Packard Science and Engineering Fellow, a Camille Dreyfus Teacher–Scholar, and an Alfred P. Sloan Fellow.

References

[1] E.J. Brown, Q. Zhang, M. Dantus, J. Chem. Phys. 110 (1998) 5772.
[2] I. Pastirk, E.J. Brown, B.I. Grimberg, V.V. Lozovoy, M. Dantus, Faraday Discuss. 113 (1999) 401.
[3] E.J. Brown, I. Pastirk, B.I. Grimberg, V.V. Lozovoy, M. Dantus, J. Chem. Phys. 111 (1999) 3779.
[4] I. Pastirk, V.V. Lozovoy, E.J. Brown, I. Grimberg, M. Dantus, J. Phys. Chem. 103 (1999) 10226.
[5] V.V. Lozovoy, B.I. Grimberg, E.J. Brown, I. Pastirk, M. Dantus, J. Raman. Spectrosc. 31 (2000) 41.
[6] V.V. Lozovoy, E.J. Brown, I. Pastirk, B.I. Grimberg, M. Dantus, in: R.J. Gordon, Y. Fujimura (Eds.), Advances in Multiphoton Processes and Spectroscopy, vol. 14, World Scientific, Singapore, 2000, pp. 62–79.
[7] V.V. Lozovoy, I. Pastirk, E.J. Brown, B.I. Grimberg, M. Dantus, Int. Rev. Phys. Chem. 19 (2000) 531.
[8] Y.R. Shen, The Principle of Nonlinear Optics, Wiley, New York, 1984.
[9] S. Mukamel, Principles of Nonlinear Optical Spectroscopy, Oxford University Press, New York, 1995.

[10] W.M. Zhang, V. Chernyak, S. Mukamel, J. Chem. Phys. 110 (1999) 5011.
[11] M.D. Fayer, Ann. Rev. Phys. Chem. 33 (1982) 63.
[12] M. Chachisvilis, H. Fidder, V. Sundström, Chem. Phys. Lett. 234 (1995) 141.
[13] M.S. Pshenichnikov, M.P. de Boeij, D.A. Wiersma, Phys. Rev. Lett. 76 (1996) 4701.
[14] R.S. Mulliken, J. Phys. Chem. 55 (1971) 288.
[15] R.G. Brewer, R.L. Shoemaker, Phys. Rev. A 6 (1972) 2001.
[16] J.P. Coffinet, F. De Martini, Phys. Rev. Lett. 22 (1969) 60.
[17] E. Yablonovitch, C. Flytzanis, N. Bloembergen, Phys. Rev. Lett. 29 (1972) 865.
[18] R.M. Hochstrasser, H.-N. Sung, J.E. Wessel, J. Chem. Phys. 58 (1973) 4694.
[19] J.E. Ivanecky, J.C. Wright, Chem. Phys. Lett. 206 (1993) 437.
[20] D.A. Blank, L.J. Kaufman, G.R. Fleming, J. Chem. Phys. 111 (1999) 3105.
[21] J.C. Kirkwood, A.C. Albrecht, J. Raman Spectrosc. 31 (2000) 107.
[22] J.I. Steinfeld, R.N. Zare, L. Jones, M. Lesk, W. Klemperer, J. Chem. Phys. 42 (1965) 25.
[23] J. Tellinghuisen, J. Quant. Spectrosc. Rad. Transf. 19 (1977) 149.
[24] S. Gerstenkorn, P. Luc, J. Physique 46 (1985) 867.
[25] I. Pastirk, V.V. Lozovoy, M. Dantus, Chem. Phys. Lett. 333 (2001) 76.
[26] B.I. Grimberg, V.V. Lozovoy, M. Dantus, S. Mukamel, J. Phys. Chem., submitted (2001).
[27] V.V. Lozovoy, I.B. Grimberg, I. Pastirk, M. Dantus, Chem. Phys. 267 (2001) in press.
[28] J.A. Leegwater, S. Mukamel, J. Chem. Phys. 101 (1994) 7388.
[29] O. Kinrot, Y. Prior, Phys. Rev. A 50 (1994) 1999.
[30] S.T. Cundiff, J.M. Shacklette, Ultrafast Phenomena XII Conference, OSA Technical Digest, Optical Society of America, Washington DC, 2000, p. 262.